Primljen / Received: 20.12.2021.
Ispravljen / Corrected: 16.8.2022.
Prihvaćen / Accepted: 18.8.2022.
Dostupno online / Available online: 10.10.2023.

Dynamic behaviour of prestressed concrete beams considering moving loads

Authors:

[1]Prof. Xuansheng Cheng
chengxuansheng@gmail.com
Corresponding author

[2]Guangyu Dong, MSc. CE
donggylut@sina.com

[1]Xianglei Wang, MSc. CE
1241576537@qq.com

[1]Liang Ma, MSc. CE
1197920722@qq.com

[2]Guoliang Li, MSc. CE
1340523276@qq.com

[1] Lanzhou University of Technology, China Ministry of Education Western Construction Disaster Risk Mitigation Center
[2] Lanzhou University of Technology, China Gansu Provincial Industrial Disaster Prevention and Mitigation Main Laboratory

Original research paper

Xuansheng Cheng, Guangyu Dong, Xianglei Wang, Liang Ma, Guoliang Li

Dynamic behaviour of prestressed concrete beams considering moving loads

Herein, the dynamic response rule of prestressed concrete beams with metal and plastic corrugated pipes with different duct grouting compactness values under moving constant concentrated loads and moving simple harmonic loads is studied. Prestressed concrete beams with metal and plastic corrugated pipes are analysed using the finite element method for the case of non-cracking. The results indicate that duct grouting compactness and forming material affect the natural vibration characteristics of prestressed concrete beams. Under identical duct grouting compactness, prestressed concrete beams with metal corrugated pipes exhibit higher frequencies compared with those with plastic corrugated pipes. The mid-span dynamic deflection of the prestressed concrete beams decreases with an increase in duct grouting compactness, which is independent of the forming material. The differences in the midspan speed and acceleration caused by the moving loads between the corrugated duct prestressed concrete beams made of metal and those made of plastic are small; this indicates that the pore-forming material has little effect on the midspan node speed and acceleration response of prestressed concrete beams.

Key words:
prestressed concrete beam, corrugated pipes, grouting compactness, nonlinear analysis, moving load, dynamic response

Izvorni znanstveni rad

Xuansheng Cheng, Guangyu Dong, Xianglei Wang, Liang Ma, Guoliang Li

Dinamičko ponašanje prednapetih betonskih greda s obzirom na pokretna opterećenja

U ovom se radu ispituje pravilo dinamičkog odziva prednapetih betonskih greda s metalnim i plastičnim valovitim cijevima različitih vrijednosti kompaktnosti injekcijske smjese kanala na pokretna konstantna koncentrirana opterećenja i pokretna jednostavna harmonijska opterećenja. Prednapete betonske grede s metalnim i plastičnim valovitim cijevima analizirane su metodom konačnih elemenata u slučajevima bez pukotina. Rezultati pokazuju da kompaktnost injekcijske smjese kanala i materijal za oblikovanje utječu na karakteristike prirodnih vibracija prednapetih betonskih greda. Pod istom kompaktnošću injekcijske smjese kanala, prednapete betonske grede s metalnim valovitim cijevima pokazuju veće frekvencije u usporedbi s onima koja imaju plastiče valovite cijevi. Dinamički progib prednapetih betonskih greda u sredini raspona smanjuje se s povećanjem kompaktnosti injekcijske smjese kanala, što je neovisno o materijalu za oblikovanje. Razlike u brzini i ubrzanju srednjeg raspona uzrokovane pokretnim opterećenjem između prednapetih betonskih greda metalnih i plastičnih valovitih cijevi su male. To pokazuje da materijal koji stvara pore ima mali učinak na brzinu čvora u sredini raspona i reakciju ubrzanja prednapetih betonskih greda.

Ključne riječi:
prednapeta betonska greda, valovite cijevi, kompaktnost injekcijske smjese, nelinearna analiza, pokretno opterećenje, dinamički odziv

1. Introduction

Owing to the continuous development of the social economy and the increasingly dense urban population distribution, three-dimensional traffic has become a mainstream direction of urban traffic development. Prestressed concrete simply supported beams are widely used in the construction of medium and small bridges owing to their simple structure and convenient construction, and thus, numerous prestressed concrete bridges have been built. With increasing traffic volume, continuous improvement in vehicle load standards, and quality problems that inevitably occur in the actual construction of prestressed concrete bridges, which affect the overall performance of bridges, the dynamic performance of prestressed concrete girder bridges has been extensively studied.

Currently, several scholars are committed to studying the mechanical properties of prestressed concrete simply supported beams. Considerable results have been achieved in numerous theoretical and experimental studies on the dynamic response of prestressed concrete beams. Li [1] studied the forced vibration of suspension bridges under the load of railway vehicles, and the vibration of arch bridges under vehicle loads. Zhang et al. [2, 3] considered the effect of track unevenness, established an analysis model of the axle system using the modal synthesis method, and analysed the entire process of high-speed trains passing through the bridge. Yang et al. [4] used the dynamic equation of a wheel-track–bridge coupling unit derived from the Hertz elastic contact model to establish the power equation of the system, and studied the dynamic response of the wheel-track–bridge coupling system. Hutton et al. [5, 6] used the finite strip method and modal analysis technology in numerous field tests to study the dynamic response of a simply supported girder bridge under the action of biaxial vehicle loads. Yang and Yin [7] proposed a finite element method to efficiently solve the vehicle-bridge coupling system. Li et al. [8] performed a foot-scale load test on a Florida highway bridge, and analysed the dynamic response of the bridge under the action of vehicle loads using a simplified finite element model of the vehicle and bridge. Li et al. [9] considered factors such as the load moving speed, beam weight, and stiffness to analyse the vertical vibration response of a prestressed concrete simply supported beam under the action of arbitrary moving loads. Shen et al. [10] studied the variation rule of the beam impact coefficient, dynamic bending moment, and dynamic shear force with the load movement velocity under different load combinations. Gao and Xu [11] used the finite element method to analyse the dynamic response of prestressed concrete simply supported beams with simultaneous static and sinusoidal loads. Yang [12] used an urban small-span prestressed concrete simple support beam as the research object, and studied the effects of the moving load velocity and bridge surface unevenness on the dynamic response of the beam using finite element analysis (FEA). Niki et al. [13] used the time-domain finite element method to numerically simulate the dynamic response of a flexible pavement to a vehicle under three-dimensional conditions. Xu et al. [14] found that vibration-reduction measures had a better vibration-reduction effect on heavy-haul railway bridges. Edgaras et al. [15] analysed the influence of deflection and crack width of a prestressed concrete beam under cyclic loading after strengthening a prestressed beam with a basalt fibre-reinforced polymer. Shi et al. [16] analysed the vehicle-bridge resonance phenomenon of double-axle trains passing through equal-span prestressed bridges to study the influence law of vehicle resonance on the vehicle-bridge system under the conditions of different vehicle speeds and different bridge spans.

In summary, numerous research results have been obtained in the study of posttensioned prestressed concrete structures; however, most studies have focused on unbonded and bonded prestressed concrete structures. Few investigations [17, 18] have studied the difference in performance between the commonly used metal and plastic corrugated pipes prestressed concrete structures in terms of the bearing capacity and use stage and did not perform a systematic comparative experimental study on them. In addition, research [19–21] on the effect of the pore-forming material and duct grouting compactness on the properties of posttensioned prestressed concrete structures is limited. However, in the actual posttensioning prestressing construction, the lack of strict sealing around the duct leads to grouting leakage, pressure grouting does not meet the requirements, and excessively large sundries and water–cement ratio, thus causing dry shrinkage; consequently, most of the duct grouting cannot meet the actual situation, which directly affect the overall performance of the bridge. Some bridges even exhibit cracks and excessive deflection after 3–6 y of usage [22–25]. To avoid this problem, the relevant duct grouting technical specifications have been specified globally, which stipulate the raw material technical requirements of grouting material and grouting agent for posttensioned prestressed concrete duct, the performance index of grouting material mixed with duct grouting material, and the construction technology of grouting and the acceptance standard of grouting quality. Two of the most widely used specifications are the European specification "Grout for prestressing tendons" (BS EN 445/446/447:2007) [26] and the United States Post-tensioning institute (PTI) specification "Specification for Grouting of post-Tensioned Structures" (PTI M55.1) [27]. The Ministry of Railways of China has also formulated the technical specifications "Technical specification of cable grouts on post-prestressed concrete railway girder" (TB/T 3192-2008) [28]. The duct grouting compactness is directly related to the durability, reliability, and safety of the prestressed concrete structure. Thus, in this study, we used the finite element method to establish the finite element model under the action of uniform moving constant loads and uniform moving harmonic loads. Next, based on the numerical analysis and comparison, the influence rules of the pore-forming material and duct grouting compactness on the dynamic response of prestressed concrete beams under the

condition of uncracking were studied, thereby providing some reference for the design, load-bearing capacity evaluation and reinforcement of prestressed concrete structures, and improving the reliability of prestressed concrete structures in the course of operation.

2. Methodology

In this study, a finite element model was established under the action of uniformly moving constant and harmonic loads to investigate the dynamic response of prestressed concrete beams. First, specimens of eight post-tensioned prestressed concrete simply supported beams were made according to the grouting compactness (full grouting, 1/3 grouting, 2/3 grouting, and without grouting) and type of corrugated pipes (metal corrugated pipes and plastic corrugated pipes). Next, prestressed concrete beams were subjected to symmetrical loading experiments at three equal points were performed to quantify the value of uniformly moving constant loads and uniformly moving harmonic loads in the FEA. Material performance tests were then performed to identify the material parameters of the prestressed concrete beams for FEA modelling. Finally, according to the parameters of the material performance tests, a finite element model of the beams was established, and a dynamic analysis under a moving load was performed. In this study, the procedure for FEA modelling was as follows.

- Prepare specimens of prestressed concrete beam for experiment
- Quantify the value of moving loads by loading experiments of prestressed concrete beams
- Identify the material parameters of the prestressed concrete beams by material performance tests
- FEA modelling.

2.1. Preparation of prestressed concrete beam specimens

Prestressed concrete beams are processed using the post-tensioning method and are widely used in bridge engineering. First, concrete was poured onto the beam, and the corrugated pipe was placed in the designated position. Second, when the strength of the concrete reached the specified limit, the stretching sequence of the steel strands was performed in batches and stages, and the error in the stretching length did not exceed 6 % of the theoretical value. Finally, the grouting volume was used to control the grouting compactness to achieve different grouting compactness values for duct grouting.

In this study, eight post-tensioned prestressed simply supported concrete beams were used. According to the grouting compactness, the metal corrugated pipe can be divided into full grouting porosity (PCB1-1), 1/3 grouting porosity (PCB1-2), 2/3 grouting porosity (PCB1-3), and without grouting porosity (PCB1-4); and the plastic corrugated pipe can be divided into full grouting porosity (PCB2-1), 1/3 grouting porosity (PCB2-2), 2/3 grouting porosity (PCB2-3), and without grouting porosity (PCB2-4). The cross-sectional dimensions were 150 mm × 250 mm, beam length was 2100 mm, and net span was 1800 mm. According to material performance tests, the compressive strength of the concrete was 40.3 MPa according to material performance tests. HRB335 grade steel bar with a diameter of 10 mm was used for the main longitudinal reinforcement, an HPB300 grade steel bar with a diameter of 6 mm was used for the stirrup, and a 1×7-2 galvanized steel strand with a nominal diameter of 6 mm was used for prestressed reinforcement. The post-tensioned force of the prestressed concrete beam was 21 kN. The diameter of the post-tensioned reserved duct was 20 mm, accounting for 0.84 % of the cross-sectional area of the beam. The dimensions and reinforcements of the beams are shown in Figure 1.

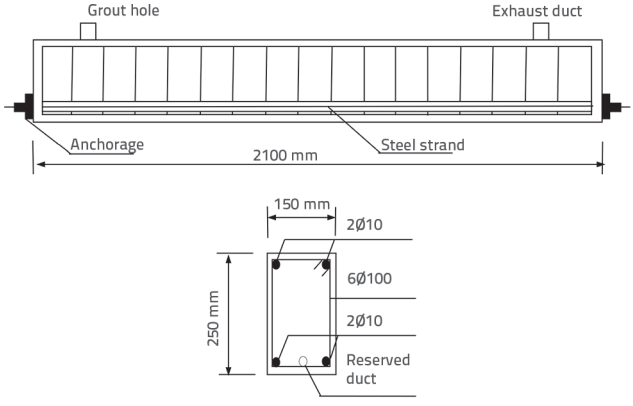

Figure 1. Dimensions and reinforcement diagram of test beams

2.2. Loading experiment of prestressed concrete beam specimens

The experimental data for the cracking and failure loads of the prestressed concrete beams under symmetrical loading at three equal points are presented in Table 1. The moving load applied to the prestressed concrete simply supported beam can be simplified using two methods [29–31]:

- the moving load is simplified to a uniform moving constant concentrated load, the mass of the moving load is ignored, and the difficulty in solving the differential equation of the variable coefficient is avoided
- considering the unevenness of the prestressed concrete beam, the moving load is simplified to a uniform moving harmonic load. To study the dynamic response of prestressed concrete beams without cracking, moving load values were selected based on the cracking load data listed in Table 1.

The minimum cracking load in Table 1 was 28.7 kN, whereas the uncracking load was 20 kN. Therefore, the moving constant concentrated load "P" was 20 kN; load moving speed "v" was 0.3, 0.5, and 0.7 m/s; moving harmonic load frequency "w"

Table 1. Measured results of bending performance of test beam

Test beam number	Metal corrugated pipe				Plastic corrugated pipe			
	PCB1-1	PCB1-2	PCB1-3	PCB1-4	PCB2-1	PCB2-2	PCB2-3	PCB2-4
Cracking load P_{cr} [kN]	31.6	36.8	42.5	45.5	28.7	31.3	35.5	43.1
Cracking displacement f_{cr} [mm]	1.61	1.92	2.15	2.35	1.41	1.52	1.84	2.06
Ultimate load P_u [kN]	79.1	86.8	93.2	103.7	77.3	81.8	87.2	96.3
Limit displacement f_u [mm]	20.38	22.03	24.46	27.20	18.01	19.82	21.21	24.96

was 1.0 Hz; load amplitude was 0.3 P = 6 kN according to the reference [30, 31], and moving harmonic load was P(t) = Pcos(ωt) = 6cos(1.0t). The moving load model is shown in Figure 2.

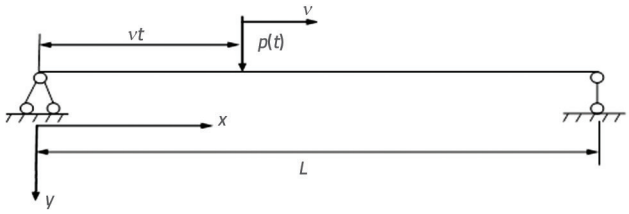

Figure 2. Moving-load mo del

2.3. Material performance tests

The material parameters of the post-tensioned prestressed concrete beams were obtained based on material performance tests. The concrete strength parameters of the beams were obtained through a compression test on a concrete cube (150 × 150 × 150 mm). Two groups of specimens were reserved during pouring of the prestressed concrete beams. Each specimen group contained three concrete cube test blocks. The curing conditions were identical to those for the prestressed concrete beams, and the curing time was 28 d. The non-prestressed bars of each specimen were the same, and two non-prestressed bars of different specifications in the same batch were reserved for testing mechanical properties, such as yield strength. The mechanical parameters of the prestressed steel strands, metal, and plastic corrugated pipes were standard values rather than those determined by testing. The material parameters are listed in Table 2. These parameters were used for the modelling and analysis.

2.4. FEA modelling

2.4.1. Units type and constitutive model

Concrete used the Solid 65 unit, generally used in the compressive capacity, which is much greater than the tensile capacity of non-uniform materials. The ordinary steel bar and prestressed reinforcement adopted the Link 8 unit; the Link 8 unit has the functions of plasticity, creep, rotation, large deformation, and large strain. The corrugated pipes used the Shell 181 unit, which is a 4-node finite strain shell unit suitable for simulating thin shell and layered structures. The bonding effect between the prestressed reinforcement and surrounding concrete was simulated using the Combin14 unit.

The Hongnestad constitutive model was used for the concrete. The non-prestressed and prestressed reinforcements used a double-straight-line constitutive model. For the pore-forming materials of the metal-corrugated pipes and plastic-corrugated pipes, an ideal elastoplastic plastic material constitutive model was used.

Table 2. Parameters of post-tensioned prestressed concrete beam

	Yield strength [MPa]	Elastic modulus [MPa]	Poisson's ratio	Density [kN/m³]
Concrete	40.3 (Uniaxial compressive strength)	3.21×10^4	0.2	25
	3.1 (Uniaxial tensile strength)			
HRB335 bars	335	2.0×10^5	0.3	78.5
HPB300 bars	300	2.1×10^5	0.3	
Prestressed steel strand	1270	2.05×10^5	0.3	77.8
Metal corrugated pipe	235	2.05×10^5	0.3	78.5
Plastic corrugated pipe	40	20	0.3	9.5

2.4.2. Simulation of bonding force between prestressed reinforcement and concrete

In the modelling process, the bonding effect between the prestressed reinforcement and concrete was simulated by adjusting the elastic coefficient of the Combin 14 unit, and the influence of the grouting quality on the beams was simulated. The duct grouting compactness model was unbonding (without grouting porosity), with an elastic constant of 10^8 (1/3 grouting porosity), elastic constant of 10^{12} (2/3 grouting porosity), and bonding (full grouting porosity).

2.4.3. Boundary conditions and application of prestress

A hinged constraint was applied to the two ends of the prestressed concrete beam, that is, the left support constraint in the X, Y, and Z directions, and the right support constraint in the Y and Z directions, to simulate the simply supported state of the beam. In FEA, the prestress simulation utilises the real strength reinforcement method, which divides the concrete and prestress reinforcement into different units and considers the action of the concrete and prestress reinforcement together. In this study, the application of prestress was realised using the initial strain method, that is, the prestressed bars themselves had a certain initial strain.

2.4.4. Model description

ANSYS was used as the finite element analysis software. The concrete and steel bars were modelled using the separation model and node coupling method, and the mesh was divided. Essentially, the concrete and steel bars were modelled and meshed separately. The beam was divided into 106 sections, and a total of 11448 concrete units were used for the entire model. In the finite element model calculation, the dead weight of the prestressed concrete beam, prestress, and load exerted on the upper part of the beam were considered. The model analysis type was structural, and the structure analysis type was transient. The finite element analysis model is shown in Figure 3.

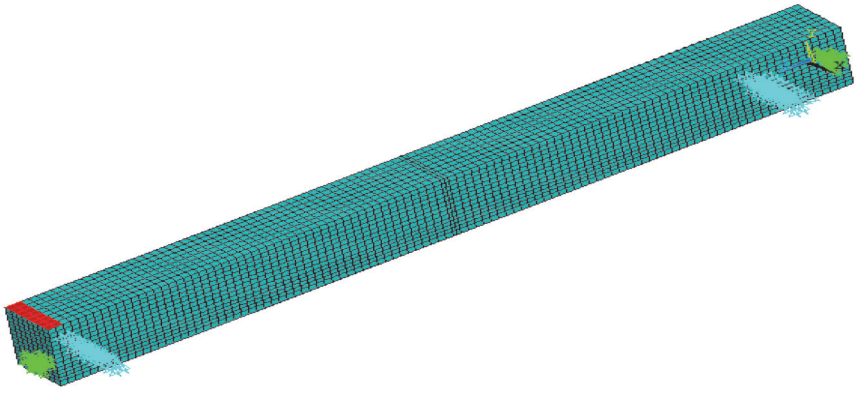

Figure 3. Finite element model

2.5. Natural frequency and vibration mode calculate theory

The finite element method was used to analyse the dynamic characteristics of simply supported prestressed concrete beams. Ultimately, this problem solves the generalised eigenvalue problem.

$$(K-\omega^2 M)\phi = 0 \quad (1)$$

where **K** is the stiffness matrix, **M** is the mass matrix, ω is the natural frequenc and ϕ is the vibrational mode.
If Eq. (1) has a nonzero solution, then

$$|K-\omega^2 M| = 0 \quad (2)$$

Eq. (2) is the characteristic equation for the structure. The subspace iteration method was used to determine the vibration mode and natural frequency of the structure.

2.6. FEA dynamic response calculate theory

The prestressed concrete simple-supported beam was discretised into a finite element set, appropriate displacement modes were selected for each element, and the kinetic energy and strain energy of each element and the entire structure were calculated. Subsequently, the vibration equation of the simply supported beam in generalised coordinates was derived from Hamilton's principle when the moving load passes uniformly. Finally, a direct integration method or mode superposition method was used. In this study, the Newmark-beta step-by-step integration method was used to discretise the motion equation in the time domain and transform it into a different scheme for time. A direct integration method was used to solve the motion equation step-by-step in the time domain.
For simply supported prestressed concrete beams, only the spatial domain is discretised; thus, the interpolation of the displacement in the element can be expressed as follows.

$$\mathbf{u} = \mathbf{N}\mathbf{u}_e \quad (3)$$

where **u** is the displacement vector of any point in the unit, **N** is the shape function matrix, and $\boldsymbol{u}_e$ is the node-displacement vector.
The strain components of each element were obtained using Eqs. (3):

$$\varepsilon = \Delta\mathbf{u} = \Delta\mathbf{N}\mathbf{u}_e = \mathbf{B}\mathbf{u}_e \quad (4)$$

where Δ is a differential operator matrix and $\boldsymbol{B}$ is a unit strain matrix.

According to Eq. (4), the stress components of each element are obtained as follows.

$$\sigma = \mathbf{D}\varepsilon = \mathbf{DBu}_e \tag{5}$$

where **D** is an elastic matrix.
The strain and kinetic energies of the element obtained by combining Eqs. (4) and (5) can be expressed as

$$\mathbf{V}_e = \frac{1}{2}\int_V \boldsymbol{\varepsilon}^T\boldsymbol{\sigma}dv = \frac{1}{2}\int_V \mathbf{u}_e^T\mathbf{B}^T\mathbf{DBu}_e dv = \frac{1}{2}\mathbf{u}_e^T\left(\int_V \mathbf{B}^T\mathbf{DB}dv\right)\mathbf{u}_e = \frac{1}{2}\mathbf{u}_e^T\mathbf{K}_e\mathbf{u}_e \tag{6}$$

$$\mathbf{T}_e = \frac{1}{2}\int_V \rho\dot{\mathbf{u}}^T\dot{\mathbf{u}}dv = \frac{1}{2}\dot{\mathbf{u}}_e^T\left(\int_V \rho\mathbf{N}^T\mathbf{N}dv\right)\dot{\mathbf{u}}_e = \frac{1}{2}\dot{\mathbf{u}}_e^T\mathbf{m}_e\dot{\mathbf{u}}_e \tag{7}$$

where $\boldsymbol{K}_e$ is the element stiffness matrix and $\boldsymbol{m}_e$ is the element uniform mass matrix.
If a volume force $\boldsymbol{q}_e$, the equivalent nodal force $\boldsymbol{R}_e$ can be obtained using the virtual work principle, which can be expressed as

$$\mathrm{R}_e = \int_V \mathrm{N}^T\mathrm{q}_e dv \tag{8}$$

If $\mathbf{q}_e$ is a viscous damping force, then the viscous damping force and equivalent nodal force are expressed as follows.

$$\mathbf{q}_{ef} = -\upsilon\dot{\mathbf{u}} = -\upsilon\mathbf{N}\dot{\mathbf{u}}_e \tag{9}$$

$$\mathbf{R}_{ef} = -\int_V \upsilon\mathbf{N}^T\mathbf{N}\dot{\mathbf{u}}_e dv = -\left(\int_V \upsilon\mathbf{N}^T\mathbf{N}dv\right)\dot{\mathbf{u}}_e = -\mathbf{C}_e\dot{\mathbf{u}}_e \tag{10}$$

The combined Eqs. (6) to (10) transform the node displacement and node force vectors in the local coordinate system into a global coordinate system using a coordinate transformation matrix. The total strain energy, total kinetic energy, and virtual work of the structure can be obtained and expressed as the sum of the total strain energy, total kinetic energy, and virtual work, as follows.

$$\mathbf{V} = \sum_{\mathbf{e}}\mathbf{V}_e = \frac{1}{2}\sum_e \mathbf{u}_e^T\mathbf{K}_e\mathbf{u}_e = \frac{1}{2}\mathbf{u}^T\left(\sum_e \mathbf{K}_e\right)\mathbf{u} = \frac{1}{2}\mathbf{u}^T\mathbf{K}\mathbf{u} \tag{11}$$

$$\mathbf{T} = \sum_{\mathbf{e}}\mathbf{T}_e = \frac{1}{2}\sum_e \dot{\mathbf{u}}_e^T m_e\dot{\mathbf{u}}_e = \frac{1}{2}\dot{\mathbf{u}}^T\left(\sum_e m_e\right)\dot{\mathbf{u}} = \frac{1}{2}\dot{\mathbf{u}}^T\mathbf{M}\dot{\mathbf{u}} \tag{12}$$

$$\delta\mathbf{W} = \sum_e \delta\mathbf{u}_e^T\left(\mathbf{R}_e + \mathbf{R}_{ef}\right) = \delta\mathbf{u}^T\left(\sum_e \mathbf{R}_e + \sum_e \mathbf{R}_{ef}\right) = \delta\mathbf{u}^T\left(\mathbf{R} + \mathbf{R}_f\right) \tag{13}$$

where $\boldsymbol{V}$ is the total strain energy; $\boldsymbol{T}$ is the total kinetic energ, δW is the sum of the virtual work of the external and damping forces, $\boldsymbol{K}$ is the structural stiffness matrix and $\boldsymbol{M}$ is the structural mass matrix.
From Eq. (10) we obtain:

$$\mathbf{R}_f = \sum_e \mathbf{R}_{ef} = -\sum_e \mathbf{C}_e\dot{\mathbf{u}}_e = -\left(\sum_e \mathbf{C}_e\right)\dot{\mathbf{u}} = -\mathbf{C}\dot{\mathbf{u}} \tag{14}$$

where **C** is the structural damping matrix.

Substituting Eq. (14) into Eq. (13), we obtain:

$$\delta\mathbf{W} = \delta\mathbf{u}^{\mathrm{T}}(\mathbf{R}\text{-}\mathbf{C}\dot{\mathbf{u}}) \tag{15}$$

The Hamilton's variational principle yields:

$$\frac{d}{dt}\frac{\partial\mathbf{T}}{\partial\dot{\mathbf{u}}_i} + \frac{\partial\mathbf{V}}{\partial\mathbf{u}_i} = \mathbf{R}_i \quad \mathrm{i} = 1, 2, \ldots, \mathrm{n} \tag{16}$$

By substituting Eqs. (11), (12), and (15) into Eq. (16), the structural vibration equation can be expressed in the global coordinate system, as follows.

$$\mathbf{M}\ddot{\mathbf{u}} + \mathbf{C}\dot{\mathbf{u}} + \mathbf{K}\mathbf{u} = \mathbf{R} \tag{17}$$

Damping matrix **C** in Eq. (17) can typically be obtained using a linear combination of the stiffness and mass matrices, which can be calculated using Eq. (18):

$$\mathbf{C} = \alpha\mathbf{M} + \beta\mathbf{K} \tag{18}$$

where α is the mass damping coefficient and β is the stiffness damping coefficient, which can be expressed by the damping ratio of any two modes and the corresponding natural frequencies:

$$\begin{cases} \alpha = \dfrac{2\left(\xi_i\omega_j - \xi_j\omega_i\right)\omega_i\omega_j}{\omega_j^2 - \omega_i^2} \\ \beta = \dfrac{2\left(\xi_j\omega_j - \xi_i\omega_i\right)}{\omega_j^2 - \omega_i^2} \end{cases} \tag{19}$$

where ω_i is the natural frequency of the first order, ω_j is the natural frequency of the second order; and ξ_i and ξ_j are the modal damping ratios of the response, which can be determined by experiment or experience and generally change in the range of 0 to 0.05 (with 0.05 for concrete structures).
For the solution of Eq. (17), the Newmark-beta step-by-step integration method can be used to obtain

$$\mathbf{u}_{t+\Delta t} = \mathbf{u}_t + \Delta t\dot{\mathbf{u}}_t + \left[\left(\frac{1}{2} - \chi\right)\ddot{\mathbf{u}}_t + \chi\ddot{\mathbf{u}}_{t+\Delta t}\right]\Delta t^2 \tag{20}$$

$$\dot{\mathbf{u}}_{t+\Delta t} = \dot{\mathbf{u}}_t + \left[(1-\gamma)\ddot{\mathbf{u}}_t + \gamma\ddot{\mathbf{u}}_{t+\Delta t}\right]\Delta t \tag{21}$$

In $\gamma \geq (1/2)$ i $\chi \geq (1/4)((1/2)+\gamma)^2$, the integral method is an unconditionally stable integral equation. Here, we used $\gamma = (1/2)$ and $\chi = (1/4)$ and converted them into the average acceleration method.
From Eqs. (20) and (21), we obtain:

$$\dot{\mathbf{u}}_{t+\Delta t} = \frac{\gamma}{\chi\Delta t}\left(\mathbf{u}_{t+\Delta t} - \mathbf{u}_t\right) + \left(1 - \frac{\gamma}{\chi}\right)\mathbf{b}_t + \left(1 - \frac{\gamma}{2\chi}\right)\Delta t\ddot{\mathbf{u}}_t \tag{22}$$

$$\ddot{\mathbf{u}}_{t+\Delta t} = \frac{1}{\chi\Delta t^2}\left(\mathbf{u}_{t+\Delta t} - \mathbf{u}_t\right) - \frac{1}{\chi\Delta t}\dot{\mathbf{u}}_t - \left(\frac{1}{2} - \chi\right)\ddot{\mathbf{u}}_t \tag{23}$$

At $t + \Delta t$, the differential equation of vibration is

$$\mathbf{M}\ddot{\mathbf{u}}_{t+\Delta t} + \mathbf{C}\dot{\mathbf{u}}_{t+\Delta t} + \mathbf{K}\mathbf{u}_{t+\Delta t} = \mathbf{R}_{t+\Delta t} \tag{24}$$

Substituting Eq. (22) and Eq. (23) into Eq. (24), we obtain

$$\begin{aligned}&\mathbf{K}\mathbf{u}_{t+\Delta t} + \frac{1}{\alpha\Delta t^2}\mathbf{u}_{t+\Delta t}\mathbf{M} + \frac{\gamma}{\chi\Delta t}\mathbf{u}_{t+\Delta t}\mathbf{C} = \mathbf{R}_{t+\Delta t}\\ &+\mathbf{M}\left[\frac{1}{\chi\Delta t^2}\mathbf{u}_t + \frac{1}{\chi\Delta t}\dot{\mathbf{u}}_t + \left(\frac{1}{2\chi} - 1\right)\ddot{\mathbf{u}}_t\right]\\ &+\mathbf{C}\left[\frac{\gamma}{\chi\Delta t}\mathbf{u}_t + \left(\frac{\gamma}{\chi} - 1\right)\dot{\mathbf{u}}_t + \left(\frac{\gamma}{2\chi} - 1\right)\Delta t\ddot{\mathbf{u}}_t\right]\end{aligned} \tag{25}$$

Eq. (25) can be used to solve $\mathbf{u}_{t+\Delta t'}$ and Eqs. (22) and (23) can be used to solve $\dot{\mathbf{u}}_{t+\Delta t}$ and $\ddot{\mathbf{u}}_{t+\Delta t}$, respectively.

3. Results analysis

3.1. Frequency analysis of prestressed concrete beams

In the vibration modal analysis of a posttensioned prestressed concrete simply supported beam, numerous order modes exist; however, the vibration characteristics of the structure are determined by the lower-order mode. Therefore, for the prestressed concrete beams of corrugated metal and plastic pipes, the modes and frequencies of the first three order modes of the prestressed concrete beams with different duct grouting compactness values were analysed and calculated. Figure 4 shows the first three order frequencies of the two different prestressed concrete beams under different duct grouting compactness values.

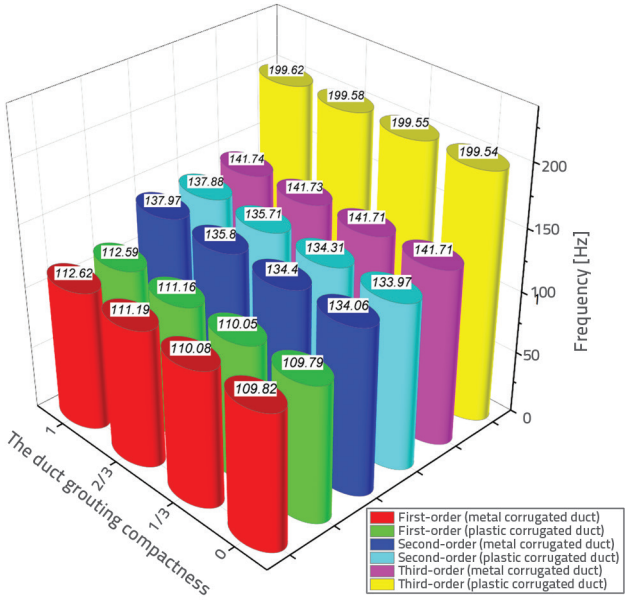

Figure 4. Grouting compactness-frequency curve

As shown in Figure 4, when the duct grouting compactness was the same, the prestressed concrete beams of the metal-corrugated pipe had a higher frequency than those of the plastic-corrugated pipe. The pore-forming materials hardly affected the first- and second-order frequencies but significantly affected the third-order frequency, thus indicating that the pore-forming material has little effect on the low-order mode shape of the prestressed concrete beam and has a significant effect on the high-order modes.

3.2. Vertical dynamic response of prestressed beams under a moving constant concentrated load

A moving constant concentrated load (P = 20 kN) was acted on the upper part of the beam, and the load moving speed was 0.3, 0.5 and 0.7 m/s to study the dynamic deflection and response rule of the mid-span speed and acceleration of the prestressed concrete beam with different grouting compactness values of metal and plastic corrugated pipes under the condition of non-cracking.

3.2.1. Dynamic deflection curve

Figure 5 shows a comparison of the dynamic deflection of prestressed concrete beams of corrugated pipes under constant loads at different speeds. The dynamic deflection peaks of each beam are shown in Figure 5.

Evidently from Figure 5, the peak value of the dynamic deflection of a simply supported beam in post-tensioned concrete exhibited a certain relationship with the moving load speed and duct grouting compactness. When the moving constant load passed over the prestressed concrete simply supported beam at different speeds, the maximum deflection of the prestressed concrete beam appeared near the mid-span position of the beam. Under the action of the constant concentrated load, with an increase in the load moving speed, the response peak value of the dynamic deflection of the beam midspan node also increased. When the load moving speed was the same, the fuller grouting of the posttensioned prestressed concrete beam orifice corresponded to a smaller dynamic deflection of the beam span. The dynamic deflection peak value without grouting porosity was at least 6 % less than that of the full grouting porosity; however, the peak value of the dynamic deflection was not significantly different when the grouting was not dense. Under the condition of the same duct grouting compactness, the dynamic deflection values of the two exhibited no distinct rule; however, the difference between the metal and plastic corrugated pipes was not significant, thus indicating that the duct material has no obvious influence on the midspan dynamic deflection of the post-tensioned concrete beam.

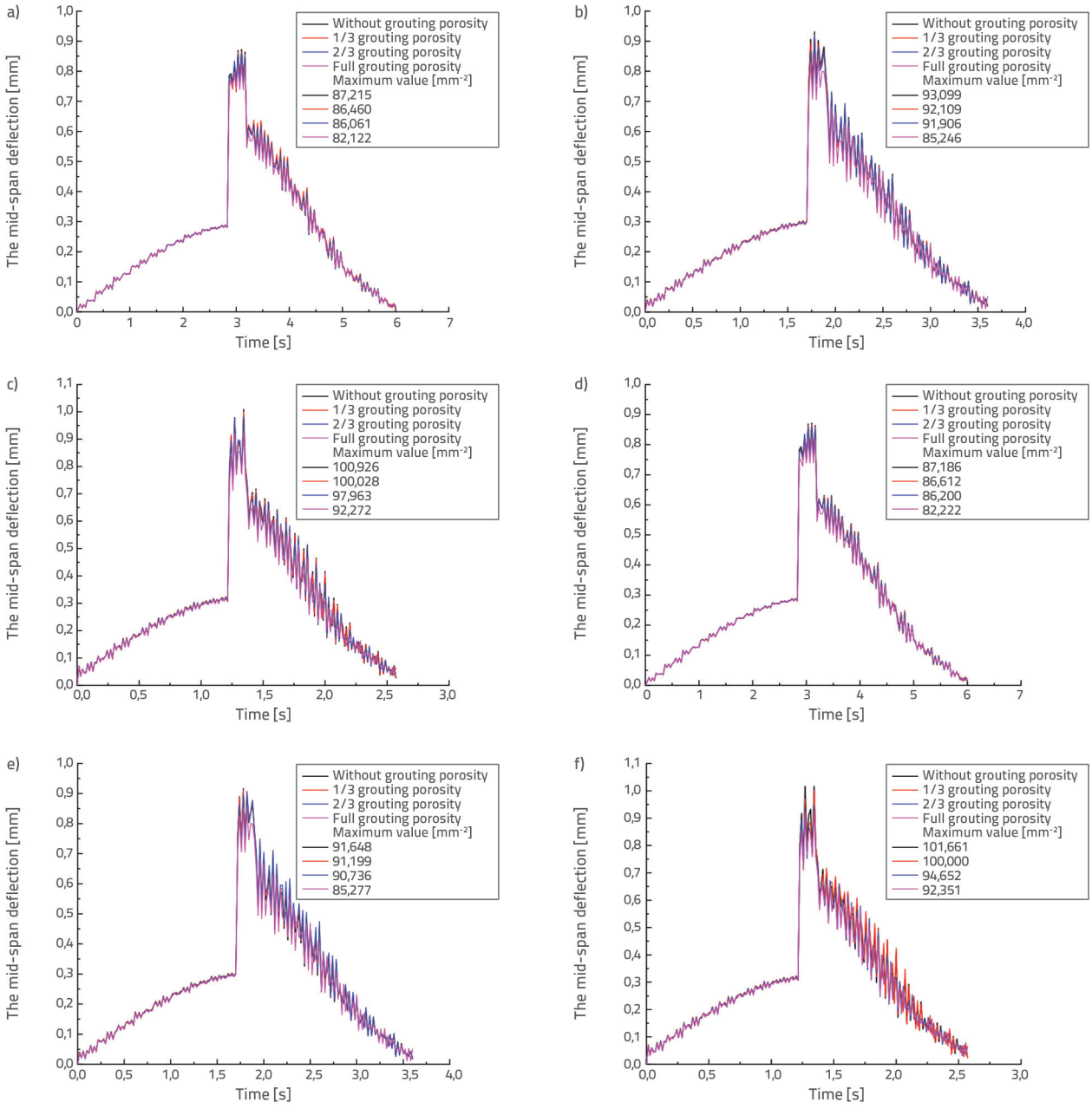

Figure 5. Dynamic deflection curve: a) Metal corrugated pipe prestressed beam v = 0.3 m/s; b) Metal corrugated pipe prestressed beam v = 0.5 m/s; c) Metal corrugated pipe prestressed beam v = 0.7 m/s; d) Plastic corrugated pipe prestressed beam v = 0.3 m/s; e) Plastic corrugated pipe prestressed beam v = 0.5 m/s; f) Plastic corrugated pipe prestressed beam v = 0.7 m/s

3.2.2. Mid-span speed and acceleration

The peak response values of the midspan speed and acceleration of the beams were calculated from the finite element results, as shown in Figures 6 and 7.

Evidently from Figures 6 and 7, with an increase in the moving speed of the load, the response peaks of the node speed and acceleration in the beam span increased. When the load moving speed was 0.3 and 0.7 m/s, with an increase in grouting compactness, the velocity and acceleration peak value of the mid-span joint of corrugated duct prestressed concrete beams made of metal and plastic gradually decreased, and the reduction amplitude reached 15–22 % and 19–29 %, respectively. When the load moving speed was 0.5 m/s, with an increase in grouting compactness, the peak velocity and acceleration of the beam midspan node both increased first and then decreased; the decrease was small. The results show that the influence of different velocities on the speed and acceleration of the beam midspan joints with different grouting compactness of the holes is different but it increases gradually

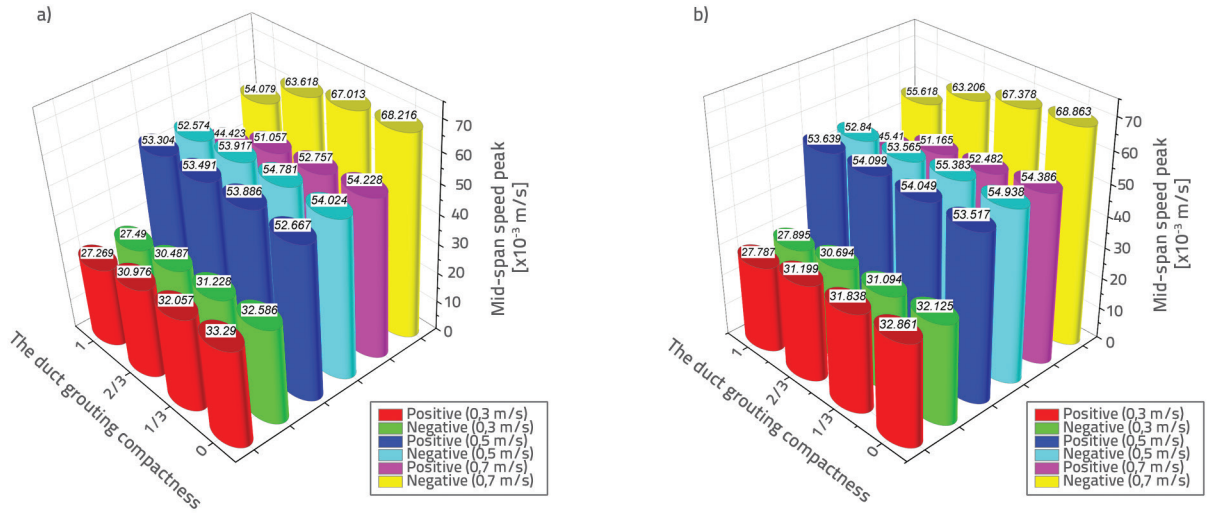

Figure 6. Mid-span speed peak of the prestressed beam (×10⁻³ m/s): a) Metal corrugated pipe prestressed beam; b) Plastic corrugated pipe prestressed beam

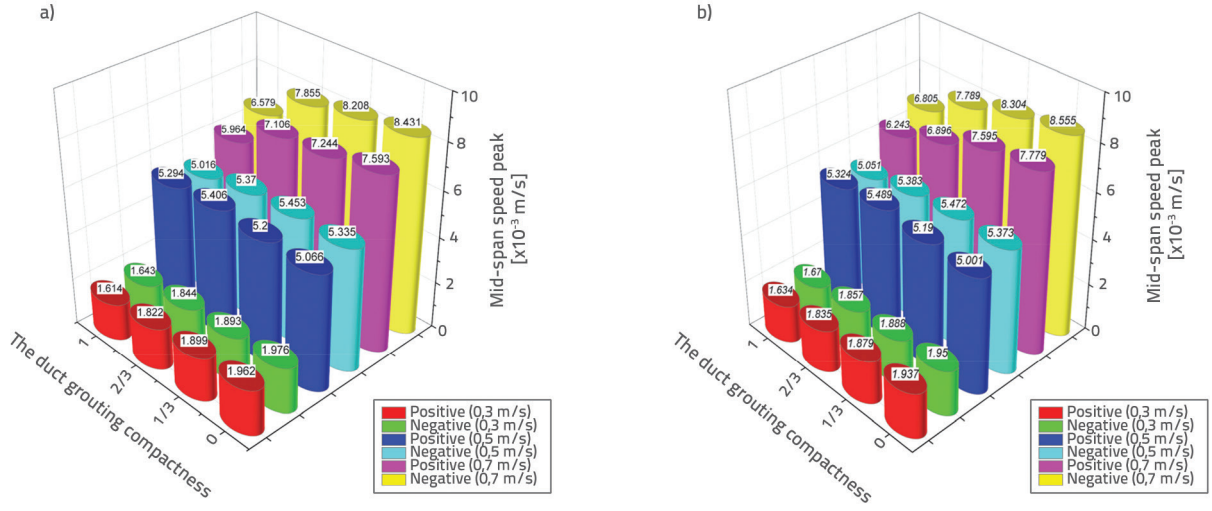

Figure 7. Mid-span acceleration peak of the prestressed beam (m/s²): a) Metal corrugated pipe prestressed beam; b) Plastic corrugated pipe prestressed beam

with an increase in velocity. However, in general, the difference in the midspan speed and acceleration caused by moving loads between corrugated duct prestressed concrete beams made of metal and plastic is small, thus indicating that the pore-forming material has little effect on the midspan node speed and acceleration response of prestressed concrete beams.

3.3. Vertical dynamic response of the prestressed beams under the moving simple harmonic load

To study the dynamic deflection and response rule of the midspan speed and acceleration of a prestressed concrete beam with different grouting compactness values of metal and plastic corrugated pipes under non-cracking conditions. The simple moving harmonic load applied to the upper part of the beam was simplified to a uniform moving harmonic load P(t) = 6cos(1.0t). The moving load vibration frequency was f = 1.0 Hz, and the load movement speeds were 0.3, 0.5, and 0.7 m/s.

3.3.1. Dynamic deflection

Figure 8 compares the dynamic deflection of the prestressed concrete beams about the corrugated pipes of two different materials under different speed moving harmonic load. The dynamic deflection peak of each beam is also shown in Figure 8.

As shown in Figure 8, the mid-span dynamic deflection curves of the posttensioned prestressed concrete simply supported beams of the two corrugated pipe materials were similar to sinusoidal curves, which vibrate at a certain frequency. When the load movement speed was low, the high-frequency fluctuation of the beam was fully developed, and the fluctuation was significant. By contrast, when the moving load speed was high, the high-frequency fluctuation of the beam could not be fully developed, and the dynamic deflection response curve was

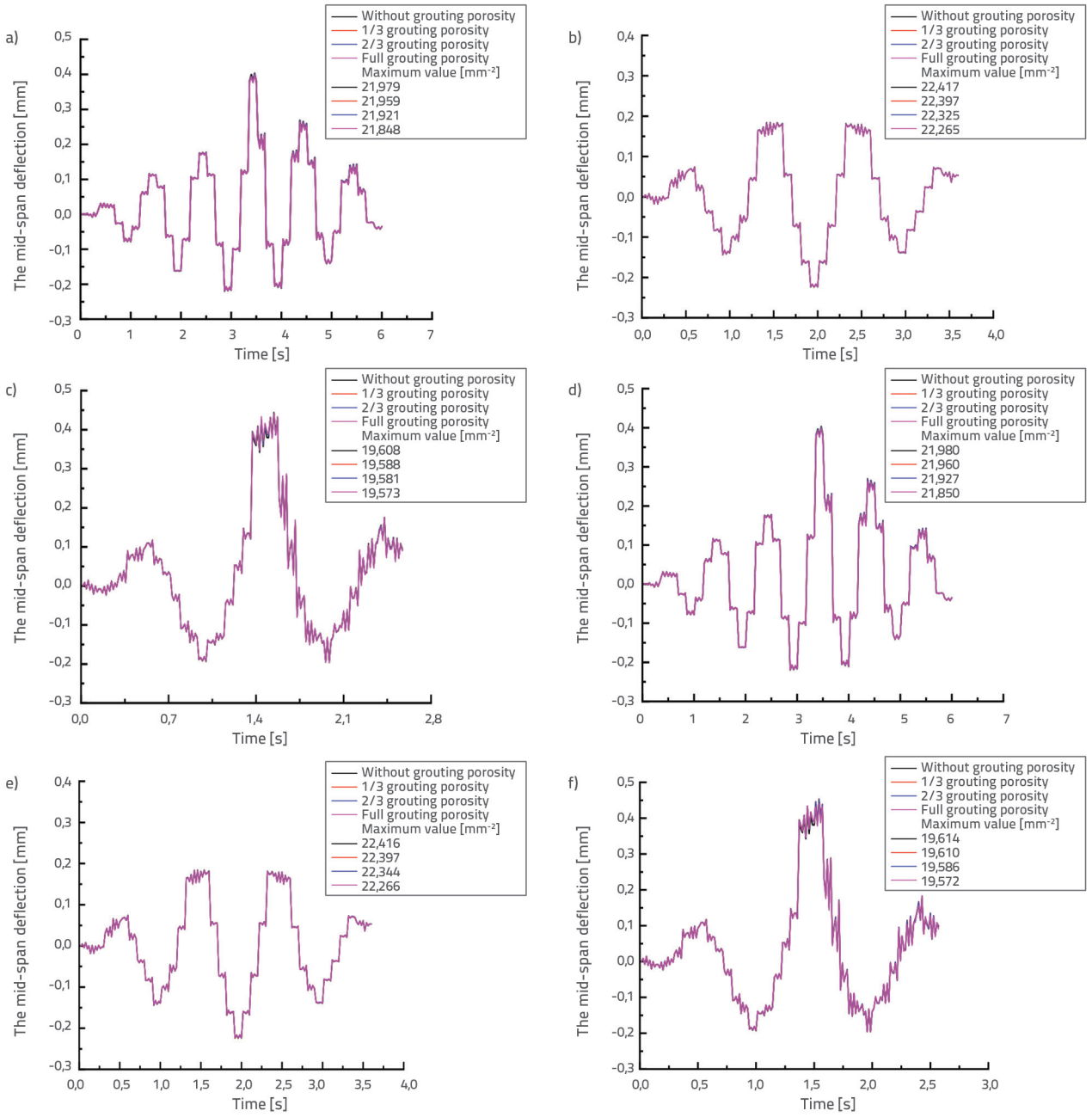

Figure 8. Dynamic deflection curve of the plastic corrugated pipe prestressed beam: a) Metal corrugated pipe prestressed beam v = 0.3 m/s; b) Metal corrugated pipe prestressed beam v = 0.5 m/s; c) Metal corrugated pipe prestressed beam v = 0.7 m/s; d) Plastic corrugated pipe prestressed beam v = 0.3 m/s; e) Plastic corrugated pipe prestressed beam v = 0.5 m/s; f) Plastic corrugated pipe prestressed beam v = 0.7 m/s

relatively smooth. At a certain load movement speed, the mid-span dynamic deflection of the prestressed concrete beam with metal and plastic corrugated ducts decreased with an increase in duct grouting compactness, thus indicating that an increase in duct grouting compactness can effectively improve the bearing capacity of the prestressed concrete beam and reduce the dynamic response of the beam. The midspan dynamic deflection of the prestressed concrete beams with metal corrugated pipes was approximately 0.02 % lower than that of the prestressed concrete beams with plastic corrugated pipes. The difference in the dynamic deflection caused by the moving harmonic load between the corrugated duct prestressed concrete beams made of metal and plastic was small, thus indicating that the pore-forming material had no significant effect on the mid-span dynamic deflection of the posttensioned prestressed beam.

3.3.2. Mid-span speed and acceleration

The peak response values for the midspan speed and acceleration of the prestressed concrete beams were calculated from the finite element results, as shown in Figures 9 and 10. Figures 9 and 10 show that with an increase in the load moving speed, the mid-span node speed peak of the prestressed concrete simply supported beam first decreased and then increased, and the acceleration peak trend increased. When the moving speed was 0.3 m/s, with an increase in duct grouting compactness, the mid-span node speed and acceleration response peaks of the prestressed concrete beams with metal and plastic corrugated ducts decreased. When the moving speed was 0.5 m/s, with an increase in duct grouting compactness, the midspan node speed and positive-acceleration response peaks of the beam gradually decreased, whereas the response peaks of the negative velocity and positive acceleration gradually increased. When the moving speed was 0.7 m/s, with an increase in duct grouting compactness, the mid-span node speed and acceleration response peaks of the beam gradually increased, thus indicating that the effect of duct grouting compactness on the mid-span node speed and acceleration response of the prestressed concrete beams is not the same under the action of a simple harmonic load. Instead, it is related to the load-moving speed, which exhibits a monotonic trend within a certain speed range. In general, the difference in the midspan speed and acceleration caused by the moving harmonic load between the corrugated duct prestressed concrete beams made of metal and plastic was small, thus indicating that the pore-forming material has little effect on the midspan node speed and acceleration response of the prestressed concrete beams.

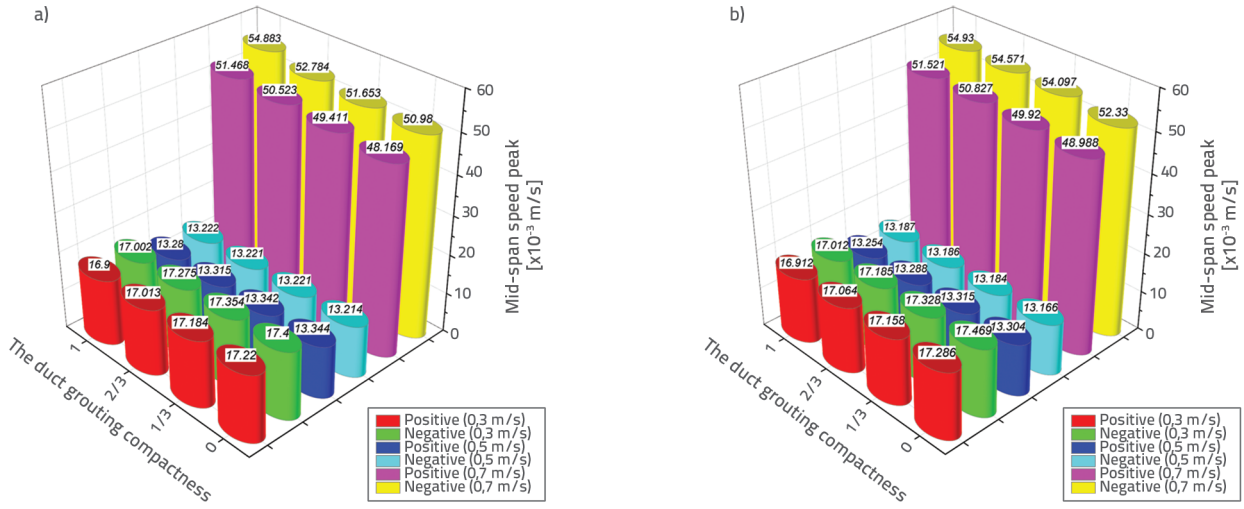

Figure 9. Mid-span speed peak of the prestressed beam (×10⁻³ m/s): a) Metal corrugated pipe prestressed beam; b) Plastic corrugated pipe prestressed beam

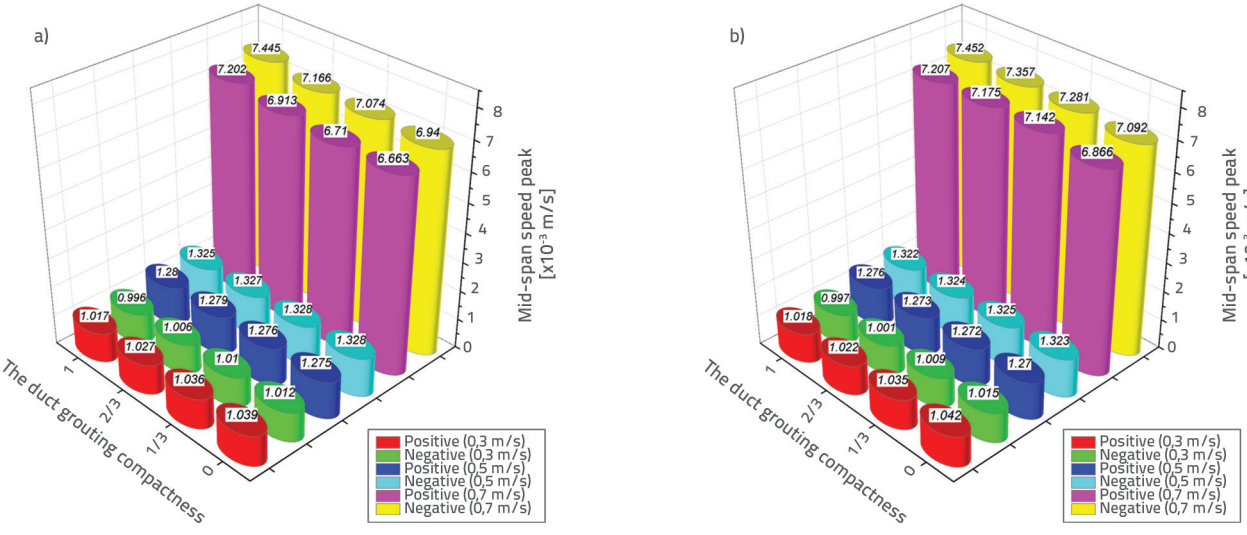

Figure 10. Mid-span acceleration peak of the prestressed beam (m/s²): a) Metal corrugated pipe prestressed beam; b) Plastic corrugated pipe prestressed beam

4. Conclusions

The duct grouting compactness affected the natural vibration characteristics of the prestressed concrete beam structure. With an increase in duct grouting compactness, the natural vibration period of the structure decreased, and the natural vibration frequency increased. When the duct grouting compactness was the same, the metal corrugated pipe prestressed concrete beams exhibited a higher frequency than the plastic corrugated pipe prestressed concrete beams, which is not evident in the first- and second-order modes but is evident in the third-order mode.

Under the action of a moving load, with an increase in duct grouting compactness, the mid-span dynamic deflection of the prestressed concrete beams decreased in the entire trend. When the moving load passed over the midspan position, the peak of the midspan cross-dynamic deflection generally appeared before and after the movements; however, it was not always observed in the middle position. Under the same moving load, the maximum dynamic deflection value appeared simultaneously, regardless of the grouting compactness of the duct and the forming material.

Under the action of a moving load, when the load moving speed was the same, the midspan node speed and acceleration peak of each beam were almost identical; this indicates that the pore-forming material has little effect on the midspan node speed and acceleration response of the prestressed concrete beams. In addition, the effects of duct grouting compactness on the mid-span node speed and acceleration of the beam were nonuniform or monotonous.

Acknowledgments

The authors gratefully acknowledge the financial support of the National Natural Science Foundation of China (Grant number: 51968045) and the Science and Technology Project of the Zhejiang Traffic Quality Supervision Bureau (Grant number: ZJ201602).

REFERENCES

[1] Li, G.H.: Stability and vibration of bridge structure, China Railway Press, Beijing, 2003.

[2] Zhang, N., Xia, H.: Dynamic analysis of railway bridge under high-speed trains, Computers & Structures, 83 (2005) 23, pp. 1891–1901, https://doi.org/10.1016/j.compstruc.2005.02.014

[3] Xia, H., Zhang, N., Gao R. et al.: Experimental study on a railway bridge and high-speed trains, Engineering Mechanics, (2007) 9, pp. 166–172.

[4] Yang, H.Y., Zhang, H.L., Chen, Z.J. et al.: Finite element analysis of train-track-bridge interaction system considering the influence of creep, China Railway Science, 34 (2013) 6, pp. 13–20.

[5] Hutton, S.G., Cheung, Y.K.: Dynamic response of single span highway bridges, Earthquake Engineering & Structural Dynamics, 7 (1979) 6, pp. 543–554, https://doi.org/10.1002/eqe.4290070604

[6] Gupta, R.K.: Dynamic loading of highway bridges, Journal of the Engineering Mechanics Division, 106 (1980) 2, pp. 377–394, 10.1061/JMCEA3.0002590

[7] Yang, Y.B., Lin, B.H.: Vehicle-bridge interaction analysis by dynamic condensation method, Journal of Structural Engineering, 121 (1995) 11, pp. 1636–1643, 10.1061/(ASCE)0733-9445(1995)121:11(1636)

[8] Li, H.Y., Wekezer, J., Kwasniewski., L.: Dynamic response of a highway bridge subjected to moving vehicles, Journal of Bridge Engineering, 13 (2008) 5, pp. 439–448, 10.1061/(ASCE)1084-0702(2008)13:5(439)

[9] Li, X.Z., Zhang, Z.J., Liu, Q.M.: Vertical dynamic response analysis of a simply supported beam bridge under successive moving loads, Journal of Vibration and Shock, 31 (2012) 20, pp. 137–142, 10.13465/j.cnki.jvs.2012.20.026

[10] Sheng, G.G., Li, C.X., Zhao, B.: Dynamic analysis of simple-supported beam subjected to moving vehicles, Engineering Mechanics, (2006) 12, pp. 154–158.

[11] Gao, Y.D., Xu, H.T., Liu, Q.L.: The finite element method of dynamic analysis on the structure of simultaneous effect of static load, Journal of Inner Mongolia University of Science and Technology, 30 (2011) 3, pp. 237–240, 10.16559/j.cnki.2095-2295.2011.03.004

[12] Yang, X.: Analysis of dynamic response and impact coefficient of beam bridge under vehicle load, 2016, Doctoral Dissertation, Chongqing Jiaotong University, Chongqing, China.

[13] Beskou, N.D., Tsinopoulos, S.V., Theodorakopoulos, D.D.: Dynamic elastic analysis of 3-D flexible pavements under moving vehicles: A unified FEM treatment, Soil Dynamics and Earthquake Engineering, (2017) 82, pp. 63–72, https://doi.org/10.1016/j.soildyn.2015.11.013

[14] Xu, J.Y., Hu J.J., Zhang, C. et al.: Vibration load identification and vibration control of bridge under heavy-haul train, Journal of Huazhong University of Science and Technology (Natural Science Edition), (2018) 2, pp. 46–50, 10.13245/j.hust.180209

[15] Atutis, E., Valivonis, J., Atutis, M.: Experimental study of concrete beams prestressed with basalt fiber reinforced polymers under cyclic load, Composite Structures, 183 (2018), pp. 389–396, https://doi.org/10.1016/j.compstruct.2017.03.106

[16] Shi, J., Yao, Z.D., Wang, Y.J.: Resonance responses of vehicle during a two-axle train passing through sequential equal-span bridges sequential equal-span bridges, Journal of Vibration and Shock, 38(2019)5, pp. 237–258, 10.13465/j.cnki.jvs.2019.05.034

[17] Cheng, H., Li, J., Lu, H.L.: Research on calculation method of bending capacity of corroded prestressed concrete Girder Bridges, World Bridges, (2015)43(01), pp. 65–68.

[18] Zhang, D.L.: Detection and research on prestressed friction Loss of corrugated duct, 2008, Masteral Dissertation, China Academy of Building Research, Beijing, China.

[19] An, L., Ji, X.B.: Research status of influence of grouting cavity on performance of post-tensioned prestressed structures, Proceedings of the Chinese Conference on Reinforcement and Evaluation of existing Bridges, (2008), pp. 67–71, https://doi.org/10.1016/S0045-7949(00)00150-4

[20] Pillai, R.G., Hueste, M.D., Gardoni, P., et al.: Time-variant service reliability of post-tensioned, segmental, concrete bridges exposed to corrosive environments, Engineering Structures, (2010) 32 (9), pp. 2596–2605, https://doi.org/10.1016/j.engstruct.2010.04.032

[21] B.H., Fu, Z.Q.: Analysis of Chinese bridge collapse accident causes in recent years, China Civil Engineering Journal, 43 (2010) S1, pp. 495–498, 10.15951/j.tmgcxb.2010.s1.010

[22] Xu, H.T., Guo, G.Z., Pu, H.L. et al.: Causes and lessons of bridge accidents in China in recent years, China Safety Science Journal, (2007) 11, pp. 90–95, 10.16265/j.cnki.issn1003-3033.2007.11.018

[23] Zhu, E.Y.: The prestressed structure of modern bridge, Tsinghua University Press, Beijing, 2012.

[24] Gao, Y.: Current status of application and research of duct grouting for prestressed concrete structure, World Bridges, (2011) 3, pp. 65–68.

[25] BS EN 445/446/447:2007.: Grout for prestressing tendons, British Standards Institution, British, 2007.

[26] PTI M55.1.: Specification for Grouting of Post-Tensioned Structures, Post-tensioning institute, United States, 2019.

[27] TB/T 3192-2008.: Technical specification of cable grouts on post-prestressed concrete railway girder, Ministry of Railways of the People's Republic of China, 2008.

[28] Zhao, J.B.: Experimental research on dynamic of pavement structure model in vehicle and pavement system, 2013, Master Dissertation, Shijiazhuang Tiedao University, Shijiazhuang, China.

[29] Zhang, D., Li, X.Z.: Analytical solution and application of vertical dynamic response of simply supported beams under the action of moving simple harmonic load, Chinese Journal of Applied Mechanics, 31 (2014) 1, pp. 144–149.

[30] Luo, J.: Determination of highway traffic load parameters of indoor test, Low Temperature Architecture Technology, 37 (2015) 3, pp. 121–123, 10.13905/j.cnki.dwjz.2015.03.046€